Research Article | Vol. 30, No. 9 / 25 Apr 2022 / Optics Express 15807
Optics EXPRESS

Diode-pumped mode-locked Yb:BaF_2 laser

Wen-Ze Xue,[1] Zhang-Lang Lin,[1] Huang-Jun Zeng,[1] Ge Zhang,[1] Pavel Loiko,[2] Liza Basyrova,[2] Abdelmjid Benayad,[2] Patrice Camy,[2] Valentin Petrov,[3] Xavier Mateos,[4] Li Wang,[3] and Weidong Chen[1,3,*]

[1]Fujian Institute of Research on the Structure of Matter, Chinese Academy of Sciences, 350002 Fuzhou, China
[2]Centre de Recherche sur les Ions, les Matériaux et la Photonique (CIMAP), UMR 6252 CEA-CNRS-ENSICAEN, Université de Caen, 6 Boulevard Maréchal Juin, 14050 Caen Cedex 4, France
[3]Max Born Institute for Nonlinear Optics and Short Pulse Spectroscopy, Max-Born-Str. 2a, 12489 Berlin, Germany
[4]Universitat Rovira i Virgili (URV), Física i Cristal·lografia de Materials (FiCMA), 43007 Tarragona, Spain
*chenweidong@fjirsm.ac.cn

Abstract: We report on a continuous-wave (CW) and passively mode-locked operation of a fluorite-type Yb:BaF_2 crystal. Pumped with a spatially single-mode, fiber-coupled InGaAs laser diode at 976 nm, the Yb:BaF_2 laser generated a maximum CW output power of 512 mW at 1054.4 nm, corresponding to a laser threshold of 36.5 mW and a slope efficiency of 65.0%. A continuous wavelength tuning across 85 nm (1007–1092 nm) was achieved. By implementing a semiconductor saturable absorber mirror for initiating and sustaining the soliton pulse shaping, near Fourier-transform-limited pulses as short as 52 fs were generated at 1058.2 nm with an average output power of 129 mW at a pulse repetition rate of ~79.5 MHz. To the best of our knowledge, this is the first report on the passively mode-locked operation of the Yb:BaF_2 crystal.

1. Introduction

Alkaline-earth fluoride crystals with a chemical formula of MF_2, where M = Ca^{2+} [1,2], Sr^{2+} [3] and Ba^{2+} [4] or their mixture [5], are attractive host materials for doping with trivalent rare-earth ions (RE^{3+}) for laser applications. They belong to the cubic class exhibiting the so-called fluorite-type structure (fluorite is the mineral form of CaF_2), sp. gr. $Fm\bar{3}m$. In RE^{3+}-doped MF_2 crystals, the charge compensation is provided by interstitial F^- anions, $M_{1-x}RE_xF_{2+x}$. There exist several possibilities for incorporation of F^- ions, so that at low doping levels (<0.1 at.%), this leads to several non-equivalent sites for the dopant ions (trigonal, C_{3v}, tetragonal, C_{4v}, cubic, O_h). With increasing the doping level, the RE^{3+} ions in MF_2 crystals tend to form clusters [6,7]. For >1 at.% doping, the majority of the ions form large clusters of different geometries. This results in profound inhomogeneous broadening of their absorption and emission bands (a "glassy-like" spectroscopic behavior).

Besides the broadband emission properties of the dopant RE^{3+} ions, the MF_2 crystals feature attractive physical properties as laser host matrices, in particular when compared to oxide crystals [8]. They exhibit broad transparency extending from the UV to the mid-IR, low refractive index, high thermal conductivity ($\kappa_0 = 9.7$ $Wm^{-1}K^{-1}$ for undoped CaF_2) with a moderate dependence on the RE^{3+} doping level, negative thermo-optic coefficients leading to weak negative thermal lensing and low phonon energies. They can also be used in the form of ceramics [9].

So far, calcium fluoride (CaF_2) is the most widespread compound of the MF_2 crystal family. Concerning laser applications, in recent years, it has been mainly studied for doping with ytterbium (Yb^{3+}) ions leading to broadband emission around 1 μm. A combination of the intrinsic features of the Yb^{3+} ion (simple energy-level scheme, low quantum defect under resonant

#459704 https://doi.org/10.1364/OE.459704
Journal © 2022 Received 4 Apr 2022; revised 13 Apr 2022; accepted 13 Apr 2022; published 22 Apr 2022

Optics EXPRESS

pumping), the smooth and broad ("*glassy-like*") emission spectra of Yb^{3+} in CaF_2, as well as the advantageous thermo-mechanical properties of the host matrix determine the high suitability of Yb:CaF_2 for the development of high-power diode-pumped femtosecond mode-locked (ML) oscillators [10–13] and amplifiers [14–17]. Sévillano *et al.* reported on a Kerr-lens mode-locked Yb:CaF_2 laser pumped by a high-brightness 979 nm fiber laser generating pulses as short as 48 fs at 1046 nm corresponding to an average output power of 2.7 W at a repetition rate of 73 MHz [18]. The longer fluorescence lifetime of Yb:CaF_2 ($^2F_{5/2}$, ~2.4 ms) ensures efficient energy storage in Q-switched lasers and ultrafast amplifiers [19]. Siebold *et al.* developed an Yb:CaF_2-based chirped-pulse amplifier delivering femtosecond laser pulses at 1032 nm with a duration of 192 fs and a pulse energy of 197 mJ, which corresponded to a terawatt-level peak power [20].

Barium fluoride (BaF_2) is another representative of the MF_2 family [21], being isostructural to CaF_2. It is commonly used for fabricating optical elements for the mid-IR part of the spectrum, as well as fast scintillators. However, less attention has been paid to its applications as a laser host matrix. It features even higher thermal conductivity ($\kappa_0 = 11.7$ $Wm^{-1}K^{-1}$ for undoped BaF_2) than its CaF_2 counterpart [4]. Camy *et al.* first reported on the continuous-wave (CW) operation of the Yb:BaF_2 crystal: pumping with a Ti:Sapphire laser at 923 nm, the maximum output power amounted to 100 mW at 1045 nm with a slope efficiency of 44% [4]. By using a Lyot filter, the spectral tuning range reached 55 nm (1006–1060 nm).

The promising spectroscopic and thermal properties of the Yb:BaF_2 crystal are attractive for the development of sub-100 fs ML lasers. We are not aware of any reports on ultrashort pulse generation using a Yb:BaF_2 crystal. In the present work, we report on the first passively ML Yb:BaF_2 laser delivering soliton pulses as short as 52 fs. Our result also represents the shortest pulse duration ever achieved from any *diode-pumped* ML Yb:MF_2-based laser.

2. Experimental setup

2.1. Crystal growth

An Yb:BaF_2 crystal was grown by the Bridgman-Stockbarger technique with RF heating. As starting reagents, we used BaF_2 and YbF_3 (purity: 4N). The initial Yb^{3+} doping level was 3 at.% (with respect to Ba^{2+}). The powders were mixed and placed in a graphite crucible. A high vacuum ($< 10^{-5}$ mbar) was created before introducing Ar and CF_4 gases to reduce oxygen pollution. The growth was performed at ~5°C below the melting point of BaF_2 of about 1400°C. The pulling rate was 1–3 mm/h. After the growth was completed, the crystal was slowly cooled down to room temperature (20°C) within 48 h. The as-grown crystal was transparent, colorless, and free of defects and inclusions, Fig. 1. The actual Yb^{3+} doping level (2.12 at.%, $N_{Yb} = 3.56 \times 10^{20}$ cm^{-3}) was determined by Inductively Coupled Plasma Mass Spectrometry (ICP-MS) leading to a segregation coefficient $K_{Yb} = 0.71$. The crystal was oriented using a Laue diffractometer.

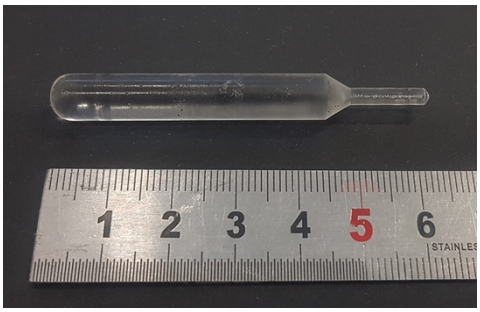

Fig. 1. A photograph of an as-grown Yb:BaF_2 crystal.

Optics EXPRESS

2.2. Optical spectroscopy

The absorption spectrum of Yb^{3+} in BaF_2 corresponding to the $^2F_{7/2} \rightarrow {}^2F_{5/2}$ transition is shown in Fig. 2(a). The maximum absorption cross-section σ_{abs} corresponding to the Yb^{3+} zero-phonon-line (ZPL) is 0.97×10^{-20} cm^2 at 975.2 nm and the corresponding absorption bandwidth (full width at half maximum, FWHM) is 5.6 nm making this crystal promising for pumping with InGaAs laser diodes. The stimulated-emission (SE) cross-section, σ_{SE}, was calculated using a combination of the reciprocity method and the Fuchtbauer–Ladenburg formula, Fig. 2(a). In the spectral range where laser operation is expected (at wavelengths well above the ZPL), $\sigma_{SE} = 0.13\times10^{-20}$ cm^2 at 1049 nm.

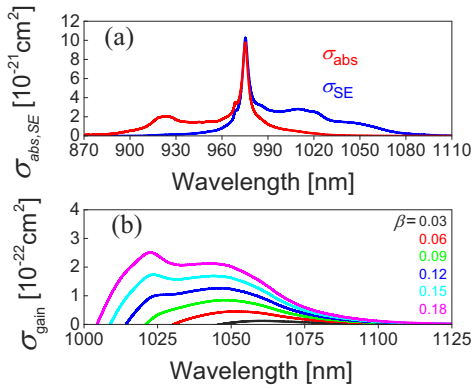

Fig. 2. Spectroscopy of Yb^{3+}:BaF_2: (a) absorption, σ_{abs}, and stimulated-emission (SE), σ_{SE}, cross-sections; (b) gain cross-sections, $\sigma_{gain} = \beta\sigma_{SE} - (1 - \beta)\sigma_{abs}$, for different inversion ratios $\beta = N_2/N_{Yb}$.

According to the quasi-three-level nature of the Yb laser scheme with reabsorption, the gain cross-section, $\sigma_{gain} = \beta\sigma_{SE} - (1 - \beta)\sigma_{abs}$, of Yb^{3+}:BaF_2 was calculated as shown in Fig. 2(b). Here, $\beta = N_2/N_{Yb}$ is the inversion ratio and N_2 is the population of the upper laser level ($^2F_{5/2}$). The gain spectra are smooth and broad (a "glassy-like" spectroscopic behavior). This is due to the strong inhomogeneous spectral broadening in all fluorite-type crystals (including BaF_2) originating from clustering of the Yb^{3+} dopant ions. With increasing the inversion ratio, the spectral maximum experiences a blue shift, from 1060 nm for small $\beta = 0.03$ to 1022 nm for high $\beta > 0.15$. The gain bandwidth (FWHM) for an intermediate $\beta = 0.12$ reaches 48 nm. This spectral behavior indicates the high potential of Yb:BaF_2 for broad wavelength tuning and sub-100 fs pulse generation from ML lasers.

The luminescence decay curve of Yb^{3+} ions in BaF_2 was measured using a finely powdered crystalline sample to avoid the effect of radiation trapping (reabsorption), Fig. 3. The Yb^{3+} ion luminescence exhibits a single-exponential decay with a characteristic lifetime $\tau_{lum} = 2.29$ ms.

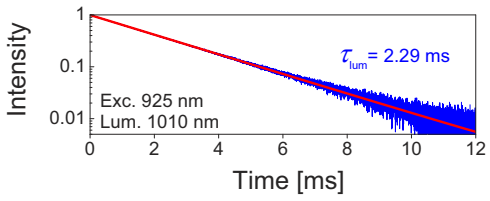

Fig. 3. The measured luminescence decay curve of the Yb:BaF_2 crystal, $\lambda_{exc} = 925$ nm, $\lambda_{lum} = 1010$ nm, *red line* – single-exponential fit.

Optics EXPRESS

Among other fluorite-type crystals, BaF_2 is known for its low phonon energy. The vibronic properties of the Yb:BaF_2 crystal were studied by Raman spectroscopy, Fig. 4. In the spectrum, a single intense peak appears centered at 242 cm^{-1} with a (FWHM) of 12 cm^{-1}. BaF_2 has a triatomic unit-cell and, therefore, it has only one first-order Raman-active mode of type F_{2g} [22]. No defect-related peaks are observed in the spectrum.

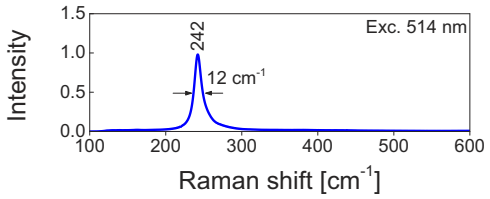

Fig. 4. Unpolarized Raman spectrum of the Yb:BaF_2 crystal, $\lambda_{exc} = 514$ nm.

2.3. Laser setup

For the laser experiments, we prepared a cubic sample cut from the as-grown Yb:BaF_2 crystal with an aperture of 3 mm × 3 mm and a thickness of 3 mm oriented along the [111] axis. It was polished to laser-grade quality from both sides and remained uncoated. The scheme of the Yb:BaF_2 laser is shown in Fig. 5. The laser crystal was mounted on a copper holder without active cooling and placed in an astigmatically compensated X-shaped standing-wave cavity between the two concave folding mirrors M_1 and M_2 (radius of curvature, RoC = -100 mm) with the Brewster minimum loss condition fulfilled for the laser wavelength. A spatially-single-mode, fiber-coupled InGaAs laser diode delivering a maximum incident power of 1.29 W (unpolarized radiation) was used as a pump source. Its emission wavelength was locked at 976 nm with a spectral linewidth (FWHM) of ~0.2 nm by using a fiber Bragg grating (FBG). The measured beam propagation factor (M^2) of the pump radiation at the maximum output power was ~1.02. The pump beam was collimated and focused into the laser crystal by using an aspherical lens L_1 (focal length: $f = 26$ mm) and an achromatic doublet lens L_2 ($f = 100$ mm) yielding a beam waist (radius) of 18.7 µm × 33.5 µm in the sagittal and tangential planes, respectively.

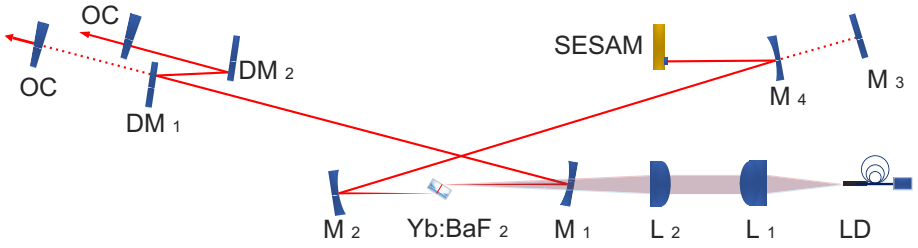

Fig. 5. Experimental configuration of the Yb:BaF_2 laser. LD: fiber-coupled InGaAs laser diode; L_1: aspherical lens; L_2: achromatic doublet lens; M_1, M_2 and M_4: curved mirrors (RoC = −100 mm); M_3: flat rear mirror for CW laser operation; DM_1 and DM_2: flat dispersive mirrors; OC: output coupler; SESAM: SEmiconductor Saturable Absorber Mirror.

A four-mirror cavity was used in the CW regime. One cavity arm was terminated by a flat rear mirror M_3 and the other arm – by a plane-wedged output coupler (OC) with a transmission at the laser wavelength T_{OC} in the 0.6% - 7.5% range. The radius of the fundamental laser mode in the Yb:BaF_2 crystal estimated using the ABCD method was 22.7 µm × 33.0 µm in the sagittal and the tangential planes, respectively. The measured single-pass pump absorption under lasing

Optics EXPRESS

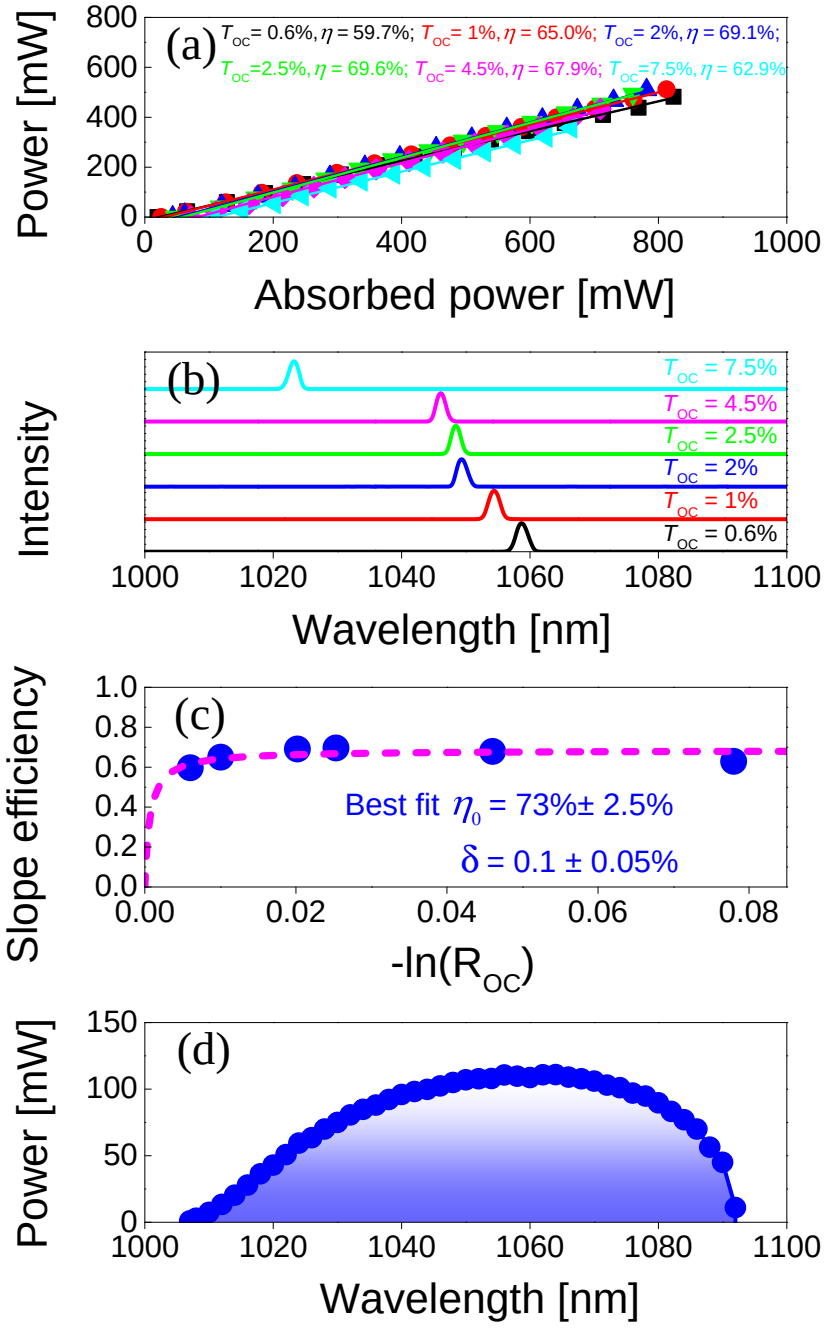

Fig. 6. CW diode-pumped Yb:BaF_2 laser: (a) input - output dependences for different OCs, η – slope efficiency; (b) typical spectra of laser emission; (c) Caird analysis: slope efficiency *vs.* $R_{OC} = 1 - T_{OC}$; (d) tuning curve obtained with a Lyot filter and $T_{OC} = 0.4\%$.

Optics EXPRESS

conditions depended on the transmission of the OC ranging from 76.7% to 81%.

For ML operation, the flat rear mirror M_3 was substituted by a curved mirror M_4 (RoC = −100 mm) for creating a second beam waist on the SESAM with a calculated beam radius of ~52 µm to ensure its efficient bleaching. Two commercial SESAMs (BATOP, GmbH) were implemented. Two flat dispersive mirrors (DM_1 and DM_2) with a negative group delay dispersion (GDD) per bounce of −250 fs^2 were introduced in the other cavity arm to compensate the material dispersion of the BaF_2 crystal (26.6 fs^2/mm at 1050 nm) and to balance the self-phase modulation (SPM) for soliton pulse shaping. The geometrical cavity length of the ML laser was 1.88 m, corresponding to a pulse repetition rate of ~79.6 MHz.

3. Continuous-wave laser operation

In the CW regime, the BaF_2 laser generated a maximum output power of 512 mW at 1054.4 nm for an absorbed pump power of 0.813 W with a laser threshold of 36.5 mW, which corresponded to a slope efficiency of 65.0% for T_{OC} = 1%, see Fig. 6(a). Slightly higher slope efficiency of 69.6% was achieved with T_{OC} = 2.5% corresponding to an output power of 493 mW at an absorbed power of 0.761 W. The laser threshold gradually increased with the output coupling, from 26.9 mW (T_{OC} = 0.6%) to 190.9 mW (T_{OC} = 7.5%). The laser wavelength experienced a monotonic blue-shift with increasing T_{OC} in the range of 1023.2–1058.7 nm, as shown in Fig. 6(b). This behavior is typical for quasi-three-level Yb lasers with inherent reabsorption at the laser wavelength.

The Caird analysis was applied by fitting the measured laser slope efficiency as a function of the output coupler reflectivity, R_{OC} = 1 - T_{OC} [23]. The total round-trip cavity losses δ (reabsorption losses excluded), as well as the intrinsic slope efficiency η_0 (accounting for the mode-matching and the quantum efficiencies) were estimated yielding $\eta_0 = 73 \pm 2.5\%$ and $\delta = 0.1 \pm 0.05\%$, as shown in Fig. 6(c). The low value of δ evidences the good optical quality of the laser crystal.

The wavelength tuning of the Yb:BaF_2 laser in the CW regime was studied by inserting a Lyot filter close to the OC (T_{OC} = 0.4%) at an incident pump power of 400 mW. The laser wavelength was continuously tunable between 1007 and 1092 nm, i.e., across 85 nm at the zero-level, Fig. 6(d).

4. Mode-locked laser operation

Initially, a SESAM with a modulation depth of 1.2% and a relaxation time of ~1 ps was implemented to start and stabilize the ML operation of the Yb:BaF_2 laser. A total round-trip negative GDD of −1000 fs^2 was introduced by using two flat DMs (DM_1 – DM_2), see Fig. 5. After careful cavity alignment, stable and self-starting ML operation was readily achieved with a 4% OC. The measured optical spectrum of the laser pulses had an emission bandwidth of 13.6 nm by assuming a $sech^2$-shaped intensity profile at a central wavelength of 1050.3 nm, see Fig. 7(a).

The recorded intensity autocorrelation trace was almost perfectly fitted with a $sech^2$-shaped temporal pulse profile giving a pulse duration (FWHM) of 87 fs corresponding to a time-bandwidth-product (TBP) of 0.322, see Fig. 7(b). An average output power of 270 mW was obtained at an absorbed pump power of 618 mW, corresponding to an optical efficiency of 43.6% and a peak power of 34.1 kW. The inset of Fig. 7(b) shows the measured intensity autocorrelation trace on a long-time span of 50 ps indicating single-pulse CW-ML operation free of multiple pulse instabilities. A radio-frequency (RF) spectrum analyzer was used for evaluating the stability of the ML operation. The relatively high extinction ratio of >74 dBc above the noise level for the first beat note at 79.59 MHz in combination with the uniform harmonics recorded on a 1-GHz frequency span are evidence for highly stable ML operation without any unwanted Q-switching or multi-pulsing instabilities, see Fig. 7(c) and (d).

Shorter pulses could be achieved by using a SESAM with higher modulation depth of 3%. With a 2.5% OC, the Yb:BaF_2 laser delivered pulses with a spectral bandwidth of 16.8 nm at a central

Optics EXPRESS

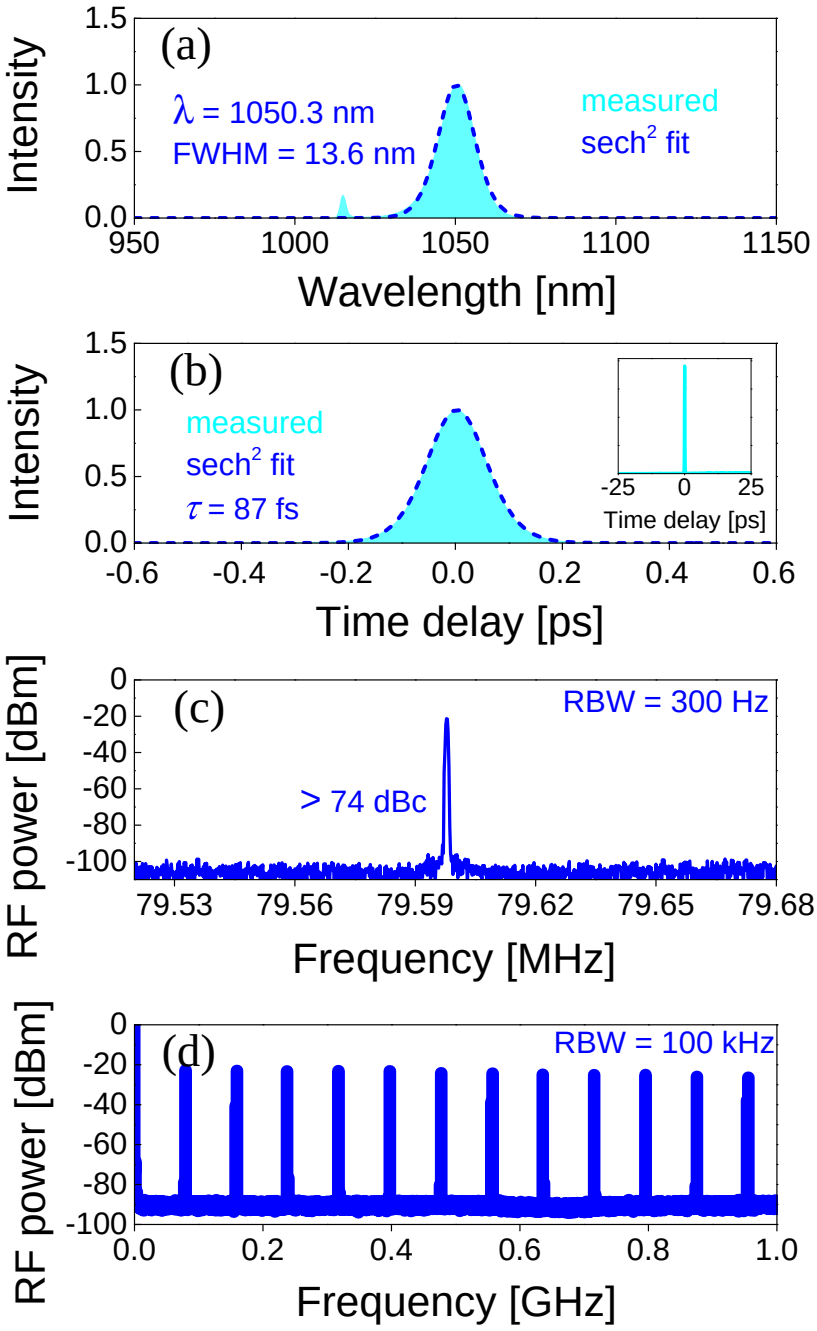

Fig. 7. SESAM ML Yb:BaF_2 laser with $T_{OC} = 4\%$. (a) Optical spectrum and (b) SHG-based intensity autocorrelation trace. *Inset*: autocorrelation trace on a time span of 50 ps. (c) First beat note at ~79.59 MHz of the RF spectrum recorded with a resolution bandwidth (RBW) of 300 Hz, and (d) RF harmonics on a 1-GHz frequency span recorded with an RBW of 100 kHz.

Optics EXPRESS

wavelength of 1053.4 nm by assuming a sech^2-shaped intensity profile, see Fig. 8(a). The almost perfect fit of the recorded intensity autocorrelation trace using a sech^2-shaped temporal intensity profile resulted in an estimated pulse duration of 70 fs, see Fig. 8(b). The 50-ps long-time scale autocorrelation trace revealed single-pulse mode-locking, see the inset of Fig. 8(b). The corresponding TBP amounted to 0.318 which was very close to the Fourier-transform-limited value of 0.315. The average output power amounted to 168 mW at an absorbed pump power of 531 mW, corresponding to an optical efficiency of 31.6% and a peak power of 26.4 kW. The measured RF spectra are shown in Fig. 8(c) and (d). Recorded at a resolution bandwidth of 300 Hz on a ~180 kHz span, the first beat note at 79.67 MHz displays an extinction ratio of >77 dBc above carrier. A 1-GHz wide-span RF measurement with an RBW of 100 kHz provided further evidence of stable single-pulse CW-ML operation.

The shortest pulses with ultimate stability were achieved with the same SESAM using a 2% OC. Assuming a sech^2-shaped spectral intensity profile, an emission bandwidth of 23 nm was obtained at a central wavelength of 1058.2 nm, see Fig. 9(a). Figure 9(b) shows the recorded intensity autocorrelation trace for the shortest pulses. The curve can be almost perfectly fitted with a sech^2-shape temporal profile, yielding an estimate of 52 fs for the pulse duration. This corresponds to a TBP of 0.320 which is only slightly above the Fourier-transform-limit. A longer time-scale intensity autocorrelation trace recorded within a 50-ps time range indicated single-pulse CW-ML operation without multi-pulsing instabilities, see inset of the Fig. 9(b). The average output power amounted to 129 mW at an absorbed pump power of 578 mW, which corresponded to an optical efficiency of 22.3% and a peak power of 27.3 kW. The RF spectra of the shortest pulses were recorded to verify the stability of the ML operation in different frequency span ranges, as shown in Fig. 9(c) and (d). The recorded fundamental beat note located at 79.54 MHz exhibited a high extinction ratio of >76 dBc above carrier. The measured uniform harmonics on a 1-GHz frequency span again revealed high stability of the single-pulse ML operation.

In order to confirm the pulse shaping mechanism, far-field beam profiles of the Yb:BaF_2 laser both in the CW and ML regimes were recorded with a IR camera placed at ~1.2 m from the OC. It was relatively easy to switch between the ML and CW laser operation regimes by a slight cavity misalignment. Almost unchanged beam diameters in the far-field were observed during such switching, see Fig. 10. The absent variation in the far-field beam profiles in combination with the nearly perfect sech^2-shaped spectral and temporal profiles of the shortest pulses indicate that soliton mode-locking was the dominant pulse shaping mechanism rather than the Kerr-lens mode-locking. This conclusion is in line with the small value of the nonlinear refractive index n_2 of BaF_2 at ~1 μm (1.4×10^{-20} m^2/W – 2.85×10^{-20} m^2/W [24]), resulting in a relatively low nonlinear amplitude modulation with the 3 mm-thick crystal.

Optics EXPRESS

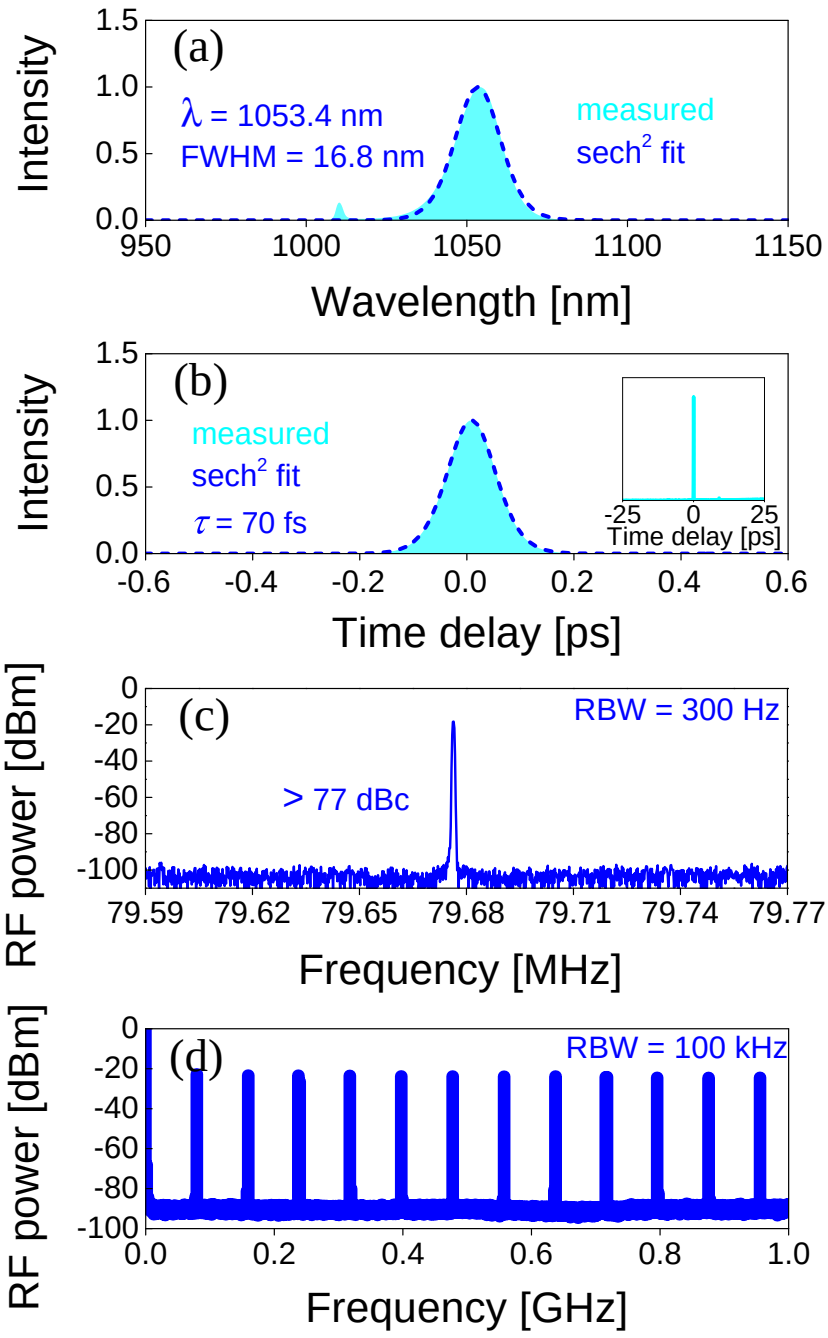

Fig. 8. SESAM ML Yb:BaF_2 laser with $T_{OC} = 2.5\%$. (a) Optical spectrum and (b) SHG-based intensity autocorrelation trace. *Inset*: autocorrelation trace on a time span of 50 ps. (c, d) RF spectra: (c) First beat note at ~79.67 MHz recorded with an RBW of 300 Hz, and (d) Harmonics on a 1-GHz frequency span recorded with an RBW of 100 kHz.

Optics EXPRESS

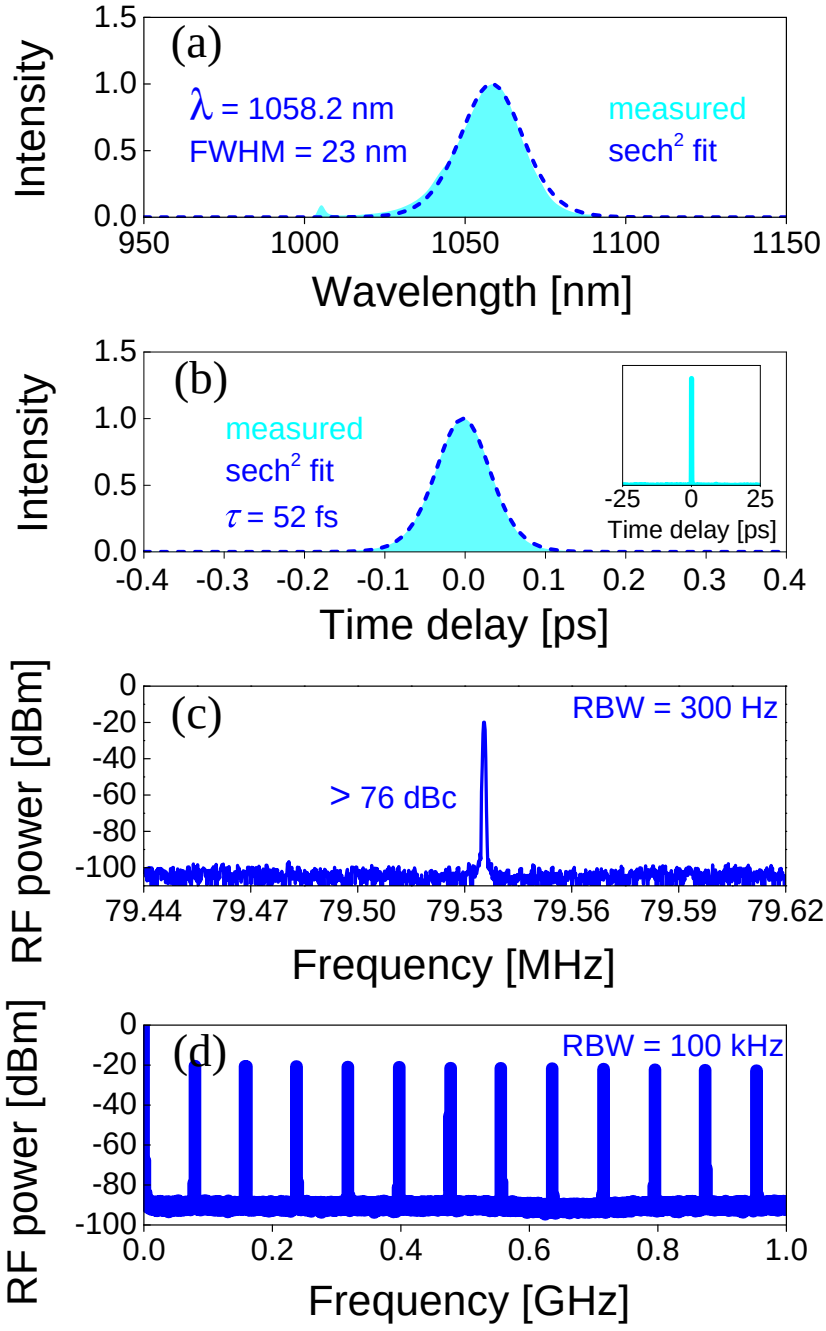

Fig. 9. SESAM ML Yb:BaF_2 laser with $T_{OC} = 2\%$. (a) Optical spectrum and (b) SHG-based intensity autocorrelation trace. *Inset*: autocorrelation trace on a time span of 50 ps. (c, d) RF spectra: (c) Fundamental beat note at 79.54 MHz recorded with an RBW of 300 Hz, and (d) Harmonics on a 1-GHz frequency span recorded with an RBW of 100 kHz.

Optics EXPRESS

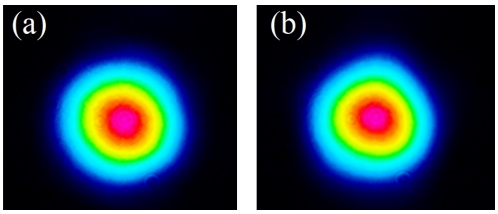

Fig. 10. Measured far-field beam profiles of the Yb:BaF_2 laser: (a) CW and (b) ML operation.

5. Conclusion

To conclude, ytterbium-doped barium fluoride (Yb:BaF_2) is a promising crystal for broadly tunable lasers and especially power-scalable ultrafast (sub-100 fs) oscillators emitting around 1 μm. It provides broad and intense absorption at the Yb^{3+} zero-phonon line facilitating its diode pumping, broad (~50 nm) and smooth gain spectra extending until 1125 nm, as well as long luminescence lifetime (2.29 ms). In the present work, we report on the first diode-pumped continuous-wave and passively mode-locked Yb:BaF_2 lasers. By using a high-brightness pump source (a cost-effective single-mode fiber-coupled InGaAs laser diode), a commercial SESAM for initiating and sustaining the mode-locked operation and a pair chirped mirrors for intracavity GDD dispersion management, soliton pulses as short as 52 fs were generated at a central wavelength of 1058.2 nm corresponding to an average output power of 129 mW at a pulse repetition rate of ~79.5 MHz. Our laser results indicate the potential of Yb:BaF_2 crystals with optimized Yb^{3+} ion doping levels and thickness for further power scaling and pulse shortening via the Kerr-lens mode-locking technique.

Funding. National Key Research and Development Program of China (2021YFB3601504); National Natural Science Foundation of China (61975208, 61905247, 61875199, U21A20508, 61850410533); Sino-German Scientist Cooperation and Exchanges Mobility Program (M-0040); Agencia Estatal de Investigación (PID2019-108543RB-I00).

Acknowledgment. Xavier Mateos acknowledges the Serra Húnter program.

Disclosures. The authors declare no conflicts of interest.

Data availability. Data underlying the results presented in this paper are not publicly available at this time but may be obtained from the authors upon reasonable request.

References

1. M. Siebold, S. Bock, U. Schramm, B. Xu, J. L. Doualan, P. Camy, and R. Moncorge, "Yb:CaF_2 - a new old laser crystal," Appl. Phys. B **97**(2), 327–338 (2009).
2. V. Petit, J. L. Doualan, P. Camy, V. Ménard, and R. Moncorgé, "CW and tunable laser operation of Yb^{3+} doped CaF_2," Appl. Phys. B **78**(6), 681–684 (2004).
3. M. Siebold, J. Hein, M. C. Kaluza, and R. Uecker, "High-peak-power tunable laser operation of Yb:SrF_2," Opt. Lett. **32**(13), 1818–1820 (2007).
4. P. Camy, J. L. Doualan, A. Benayad, M. Von Edlinger, V. Ménard, and R. Moncorgé, "Comparative spectroscopic and laser properties of Yb^{3+}-doped CaF_2, SrF_2 and BaF_2 single crystals," Appl. Phys. B **89**(4), 539–542 (2007).
5. J. L. Doualan, P. Camy, A. Benayad, V. Ménard, R. Moncorgé, J. Boudeile, F. Druon, F. Balembois, and P. Georges, "Yb^{3+} doped (Ca, Sr, Ba)F_2 for high power laser applications," Laser Phys. **20**(2), 533–536 (2010).
6. V. Petit, P. Camy, J.-L. Doualan, X. Portier, and R. Moncorgé, "Spectroscopy of Yb^{3+}:CaF_2: from isolated centers to clusters," Phys. Rev. B **78**(8), 085131 (2008).
7. B. Lacroix, C. Genevois, J. L. Doualan, G. Brasse, A. Braud, P. Ruterana, P. Camy, E. Talbot, R. Moncorgé, and J. Margerie, "Direct imaging of rare-earth ion clusters in Yb:CaF_2," Phys. Rev. B **90**(12), 125124 (2014).
8. F. Druon, S. Ricaud, D. N. Papadopoulos, A. Pellegrina, P. Camy, J. L. Doualan, R. Moncorgé, A. Courjaud, E. Mottay, and P. Georges, "On Yb:CaF_2 and Yb:SrF_2: review of spectroscopic and thermal properties and their impact on femtosecond and high power laser performance," Opt. Mater. Express **1**(3), 489–502 (2011).
9. P. Aballea, A. Suganuma, F. Druon, J. Hostalrich, P. Georges, P. Gredin, and M. Mortier, "Laser performance of diode-pumped Yb:CaF_2 optical ceramics synthesized using an energy-efficient process," Optica **2**(4), 288–291 (2015).

Optics EXPRESS

10. F. Friebel, F. Druon, J. Boudeile, D. N. Papadopoulos, M. Hanna, P. Georges, P. Camy, J. L. Doualan, A. Benayad, R. Moncorge, C. Cassagne, and G. Boudebs, "Diode-pumped 99 fs Yb:CaF_2 oscillator," Opt. Lett. **34**(9), 1474–1476 (2009).
11. G. Machinet, P. Sevillano, F. Guichard, R. Dubrasquet, P. Camy, J. L. Doualan, R. Moncorgé, P. Georges, F. Druon, D. Descamps, and E. Cormier, "High-brightness fiber laser-pumped 68 fs-2.3 W Kerr-lens mode-locked Yb:CaF_2 oscillator," Opt. Lett. **38**(20), 4008–4010 (2013).
12. F. Druon, D. N. Papadopoulos, J. Boudeile, M. Hanna, P. Georges, A. Benayad, P. Camy, J. L. Doualan, V. Menard, and R. Moncorge, "Mode-locked operation of a diode-pumped femtosecond Yb:SrF_2 laser," Opt. Lett. **34**(15), 2354–2356 (2009).
13. A. Lucca, G. Debourg, M. Jacquemet, F. Druon, F. Balembois, P. Georges, P. Camy, J. L. Doualan, and R. Moncorge, "High-power diode-pumped Yb^{3+}:CaF_2 femtosecond laser," Opt. Lett. **29**(23), 2767–2769 (2004).
14. G. Machinet, G. Andriukaitis, P. Sévillano, J. Lhermite, D. Descamps, A. Pugžlys, A. Baltuška, and E. Cormier, "High-gain amplification in Yb:CaF_2 crystals pumped by a high-brightness Yb-doped 976 nm fiber laser," Appl. Phys. B **111**(3), 495–500 (2013).
15. D. N. Papadopoulos, F. Friebel, A. Pellegrina, M. Hanna, P. Camy, J. L. Doualan, R. Moncorge, P. Georges, and F. P. H. J. Druon, "High repetition rate Yb:CaF_2 multipass amplifiers operating in the 100-mJ range," IEEE J. Sel. Top. Quantum Electron. **21**(1), 464–474 (2015).
16. F. Druon, K. Genevrier, P. Georges, and D. N. Papadopoulos, "Comparison of multi-pass and regenerative strategies for energetic high-gain amplifiers based on Yb:CaF_2," Opt. Lett. **45**(16), 4408–4411 (2020).
17. S. Ricaud, P. Georges, P. Camy, J. L. Doualan, R. Moncorge, A. Courjaud, E. Mottay, and F. Druon, "Diode-pumped regenerative Yb:SrF_2 amplifier," Appl. Phys. B **106**(4), 823–827 (2012).
18. P. Sevillano, G. Machinet, R. Dubrasquet, P. Camy, J. L. Doualan, R. Moncorge, P. Georges, F. P. Druon, D. Descamps, E. E. D. H. G. Cormier, and P. Moulton, "Sub-50 fs, Kerr-lens mode-locked Yb:CaF2 laser oscillator delivering up to 2.7 W," in *Advanced Solid-State Lasers Congress* (Optical Society of America, Paris), p. AF3A.6 (2013).
19. S. Ricaud, F. Druon, D. N. Papadopoulos, P. Camy, J. L. Doualan, R. Moncorge, M. Delaigue, Y. Zaouter, A. Courjaud, P. Georges, and E. Mottay, "Short-pulse and high-repetition-rate diode-pumped Yb:CaF_2 regenerative amplifier," Opt. Lett. **35**(14), 2415–2417 (2010).
20. M. Siebold, M. Hornung, R. Boedefeld, S. Podleska, S. Klingebiel, C. Wandt, F. Krausz, S. Karsch, R. Uecker, A. Jochmann, J. Hein, and M. C. Kaluza, "Terawatt diode-pumped Yb:CaF_2 laser," Opt. Lett. **33**(23), 2770–2772 (2008).
21. I. H. Malitson, "Refractive properties of barium fluoride," J. Opt. Soc. Am. **54**(5), 628–632 (1964).
22. A. R. Gee, D. C. O'Shea, and H. Z. Cummins, "Raman scattering and fluorescence in calcium fluoride," Solid-State Commun. **4**(1), 43–46 (1966).
23. J. A. Caird, S. A. Payne, P. Staber, A. Ramponi, L. Chase, and W. F. Krupke, "Quantum electronic-properties of the $Na_3Ga_2Li_3F_{12}$:Cr^{3+} laser," IEEE J. Quantum Electron. **24**(6), 1077–1099 (1988).
24. T. R. Ensley and N. K. Bambha, "Ultrafast nonlinear refraction measurements of infrared transmitting materials in the mid-wave infrared," Opt. Express **27**(26), 37940–37951 (2019).